Chemical Engineering Journal 155 (2009) 361–370

Contents lists available at ScienceDirect

Chemical Engineering Journal

journal homepage: www.elsevier.com/locate/cej

Extremely simple pressure regulator – computation studies

V. Tesař*

Department of Thermodynamics, Institute of Thermomechanics, v.v.i. Academy of Sciences of the Czech Republic, Dolejskova 5, 182 00 Prague, Czech Republic

ARTICLE INFO

Article history:
Received 29 May 2009
Received in revised form 27 June 2009
Accepted 7 July 2009

Keywords:
Fluidics
Pressure regulation
Passive regulator
Loading characteristic

ABSTRACT

Numerical flowfield computation studies were performed to obtain qualitative understanding of the pressure regulating mechanism of the simplest pressure regulator – an almost unknown no-moving-part fluidic device capable of keeping a constant pressure difference across a load in spite of the hydraulic properties of the latter varying in a wide range. Two application examples are discussed. In one of them, the load is a box, in which the regulator sized in hundreds of millimetres maintains pressurised atmosphere. In the other case, a millimetre-sized regulator is made as an integral part of a microfluidic circuit. Due to the purely empirical way in which the regulator geometry was developed, there has been no clear idea about its functioning. The computations run to obtain an insight into the pressure-keeping effect indicate an unexpected considerable flowfield three-dimensionality (despite the nominally two-dimensional geometry) and an essential role of a recently identified (Tesař, 2009) pressure recovery mechanism.

1. Introduction

1.1. The task

Maintaining operational conditions, pressure being among them a very important one, is a task requested very often in chemical engineering. Accordingly, a vast number of pressure regulators are offered on the market (e.g., [1]), starting from the classical versions with mechanical feedback between a pressure-sensing membrane and a mechanical flow-control valve and ending at electronic circuit versions with semi-conductor pressure sensors and the valve driven by an electric servomechanism. None of these versions are really inexpensive. In addition, their disadvantages are the considerable volume they occupy and, despite their generally good reliability record, the possibility of malfunctioning due to membrane or spring rupture or seizing of the moving parts.

There are two main reasons that may require pressure regulation in a system (Table 1). In the case discussed here, it is assumed that a fluid flow passes through a load – such as, e.g., a microreactor – the hydrodynamic properties of which vary, resulting without the regulator in excursions from the desirable pressure levels. The task of the regulator is to maintain constant the pressure difference across this load. The change in the pressure without the regulator depends on the loading characteristic of the fluid flow source. The regulator placed between the source and the load changes, in effect, the characteristic so that its shape is flat horizontal so that at all operating conditions the pressure remains the same.

1.2. Open-loop regulator with fixed-geometry cavity

An extremely simple solution to the regulator question discussed in the present paper is the fluidic device according to ref. [2]. In the absence of a feedback loop control, the pressure may not be kept perfectly constant, but it certainly avoids large pressure excursions which is what is really required in majority of cases. The operation without any pressure sensor or feedback control loop means the regulating effect depends wholly on the internal aerodynamics. The geometry of this device was developed in mid-1970 of the last century [2,3]. Unfortunately, since then it remained practically unknown. It exhibits an almost perfectly flat loading characteristic, with extreme pressure excursions typically less than 1–2% even with vast variations of the load connected to its terminals. Containing no moving or elastically deformed components and consisting of only quite simple-shaped fixed-geometry cavities, this regulator device is easily manufactured. It may be even made by etching in a chip as an integral part of a microfluidic circuit in which the pressure is regulated. There is nothing that could possibly break or seize, thus exhibiting a permanent, maintenance-free reliability. It is robust, resistant to vibration, to high temperature (since, because of the simple geometry, it may be made from refractory material), and is not prone to being impaired or damaged by overloading.

The geometry of the device was originally [3] developed by an empirical procedure of gradual adjustment of shape details of the internal cavity. The success of the pressure-maintaining capability was later verified independently by other researchers (e.g., [4]). Nevertheless, the precise reasons for the pressure-keeping mechanism of the geometry as simple as that presented in Fig. 1 remained until now rather enigmatic.

* Tel.: +420 2 6605 2270.
E-mail address: tesar@it.cas.cz.

1385-8947/$ – see front matter © 2009 Elsevier B.V. All rights reserved.
doi:10.1016/j.cej.2009.07.048

Nomenclature

b	nozzle width (m)
e_V	fluid specific energy in terminal V (m^2/s^2)
e_Y	fluid specific energy in terminal Y (m^2/s^2)
h	depth of cavities (m)
$\dot{M}$	mass flow rate (kg/s)
$\dot{M}_Y$	mass flow rate (kg/s)
$\dot{M}_S$	mass flow rate (kg/s)
P	pressure (Pa)
P_S	pressure in the supply terminal S (Pa)
P_V	pressure in the vent terminal V (Pa)
P_Y	pressure in the output terminal Y (Pa)
Re	Reynolds number (–)
s	splitter distance (m)
X_1	axial distance (m)

Greek letters

Δe	specific energy drop (m^2/s^2)
ΔP	pressure drop across the load (Pa)
ΔP_S	pressure drop between terminals S and V (Pa)
ΔP_Y	pressure drop between terminals Y and V (Pa)
λ	aspect ratio (–)
μ	relative flow rate (–)
μ_Y	relative control flow rate (–)
π	relative pressure difference (–)
π_S	relative supply pressure difference (–)
π_Y	relative output pressure difference (–)

1.3. Example: protective pressurisation

Because of their tiny dimensions, channels of modern microfluidic devices – such as, among others, chemical microreactors used in parallel tests in combinatorial chemistry [5] – may be easily clogged by foreign objects of the size so small that they would cause no problems whatsoever in other branches of engineering. Quite dangerous may be dust or aerosol particles carried by surrounding air. The microdevices have to be supplied with carefully filtered fluids and if it is necessary to access their internal cavities – e.g., for changing the contents of heterogeneous catalyst inside the microreactor – the operation has to be made in a protective atmosphere, usually at an increased pressure.

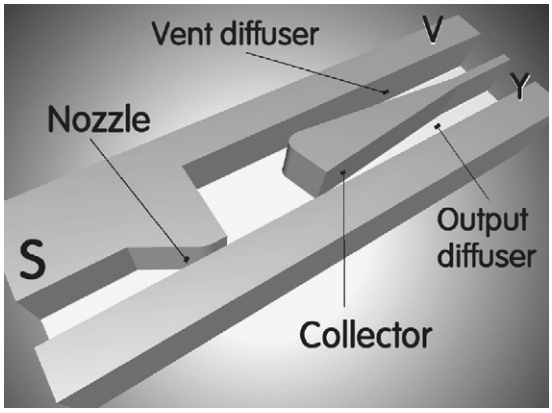

Fig. 1. The pressure regulating cavities according to ref. [2]. Fluid is supplied into S, the load is connected between the two exit terminals Y (output) and V (vent), the latter open to the common terminal – atmosphere (when working with air) or to the main tank (in the case of liquid).

Experience with simple pressurisation by a blower as shown in Fig. 2 has been, unfortunately, rather unpleasant. The blower must be dimensioned so as to provide a sufficient pressure difference ΔP_b (Fig. 3) even in the situations occurring, e.g., after opening the access door or the glove being torn.

Because of the typical shape of the blower loading characteristics (the dependences of the generated pressure difference – or more generally difference in specific energy Δe of the fluid – on the air flow rate), as presented in Fig. 3, the pressure difference between the box and the atmosphere increases to unpleasant and, indeed, potentially dangerous levels ΔP_a if the box is fully closed. The sloping shape of the characteristic is, of course, the consequence of inevitable hydraulic losses both in the blower as well as in other components of the system. As the flow rate decreases, the effect of these losses ceases to be felt and the pressure can reach inconvenient magnitudes.

Table 1
The task of a pressure regulator is to suppress the variation of the conditions in the load, which arise due to either one of the causes A or B. The fluidic regulator device discussed here is intended to eliminate the cause A by changing the source characteristic into a horizontal line, so that all the intersection points lie at ΔP_{load} = const.

Alternative causes of pressure variations across the load	
A	B
Varied hydrodynamic properties of the load	Variations in the fluid source
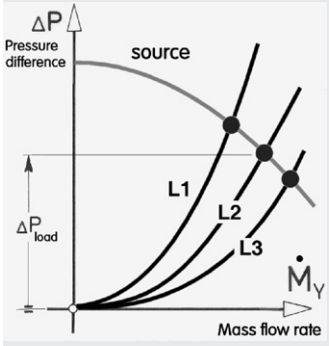	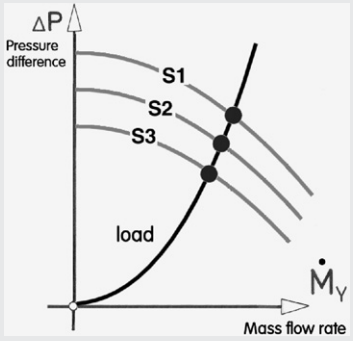
Characteristics of the load vary – e.g., by increasing the size of the cross-sectional area available for the fluid flow. With three different areas – leading to the three load characteristics, L1, L2, and L3 – three different values of the pressure drop across the load ΔP_{load} are obtained at the relevant intersections with the characteristic of the fluid source (e.g., a pump)	Characteristics of the fluid source – e.g., a pump – vary, e.g., due to opening or closing a flowpath into other loads. With three different source characteristics, S1, S2, and S3 – three different values of the pressure drop across the load are obtained at the intersections with the characteristic of the load (e.g., a chemical reactor)

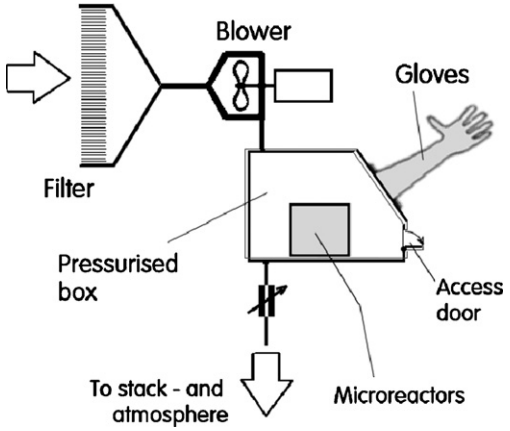

Fig. 2. Schematic representation of glove box with test microreactors (opened between operation runs, e.g., for insertion of alternative heterogeneous catalysts) with non-regulated protective pressurisation. Between uses, the gloves are inflated inner-side out.

Some blowers may even exhibit at the small flow rates the surging behaviour, but even without it the high pressure causes problems. It stresses mechanically the acrylic glass typically used for windows in the box walls and may cause them to break. Also the gloves have to be chosen thicker to withstand the maximum possible pressure difference. Their thickness makes them less convenient for use – especially leading to loss of tactile sensitivity at fingertips. When the access door is open, the high internal pressure can cause smaller object in the box to move undesirably towards the exit. All these reasons call for providing the protective boxes with a pressure regulator. This increases unduly the box price and the regulator complexity can make it less reliable. Sometimes boxes are not provided by individual blowers but connected to the common pressurised air distribution net. Dangerous situations may arise if the regulator stops operating in the case of electric current failure while the pressure in the net is still present.

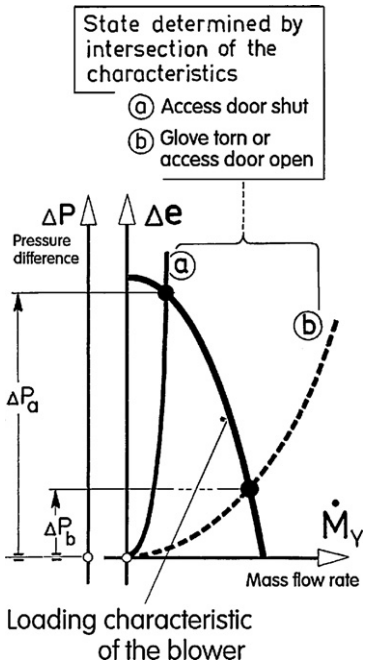

Fig. 3. To obtain the minimum necessary pressurisation in the regime (b), typical shape of the blower characteristic, without pressure regulator, causes a dangerously high pressure (stressing the walls of the protective box and gloves) in the regime (a).

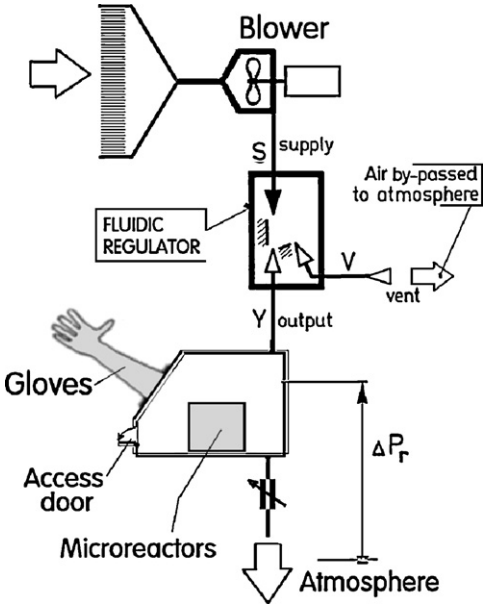

Fig. 4. Insertion of the fluidic regulator into the glove box from Fig. 2 in effect flattens the loading characteristic of the pressurised air source, thus maintaining the constant pressure ΔP_r between the protective box and the atmosphere, irrespective of opening or closing the access door or a damage to a glove.

All these disadvantages are removed by using the described no-moving-part pressure regulator as shown in Fig. 1, made at a small cost from sheet metal at the size of the order of 10^2 mm, placed between the pressurised air source and the glove boxes (Fig. 4). The flat shape of the loading characteristic, as shown in Fig. 5, maintains the constant pressure difference ΔP_r between the internal space of the box and atmosphere under all conditions.

1.4. Another application example

Because the described regulators were found to operate successfully at low Reynolds numbers, typically of the order of Re ~1000, they could be used to maintain constant pressure conditions in pressure-driven microfluidic systems [6]. In this case, the

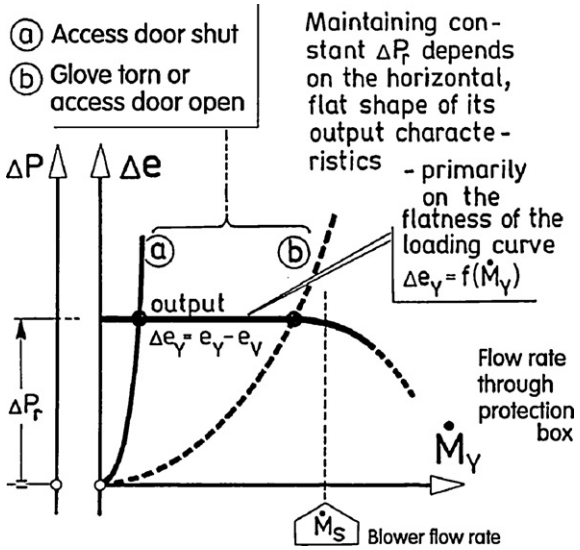

Fig. 5. Graphical presentation (to be compared with Fig. 3) of the consequences of the flat shape of the loading characteristic.

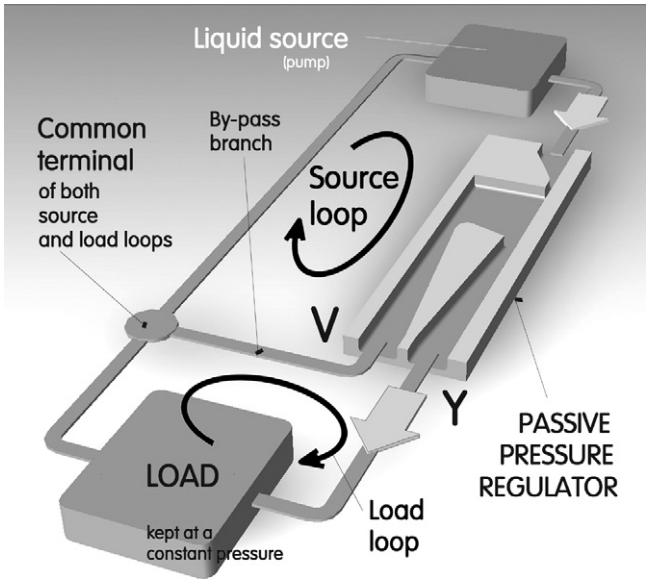

Fig. 6. The discussed fluidic pressure regulator operates between two fluid flow circuit loops: the source loop containing the pump (or other fluid source) and the load loop containing the load with controlled pressurisation.

pressure is kept constant by the hydrodynamic phenomena taking place inside the cavity positioned upstream from the pressure-sensitive device. The basic principle of circuit design based on the Kirchoff's concervation laws for circuit nodes and loops [14] is directly applicable according to Fig. 6. As shown in Figs. 7 and 9, this pressure-keeping cavity with two diffuser-shaped outlets may be made by etching integrally in a single manufacturing step together with other channels and cavities of the system. It should be noted that in the case shown in Fig. 4, the atmosphere represented the common terminal of Fig. 6, belonging to both fluidic circuit loops between which the regulator is positioned. With a chemical reactor (Fig. 7), varying the character of the fluids, the basic principle of the circuit design may be even more difficult to recognise – especially if, as shown in Fig. 8, there are more fluids in the circuit. Fig. 9 presents an example of a typical application in biomedical microfluidics (keeping pressure-sensitive captive biological objects).

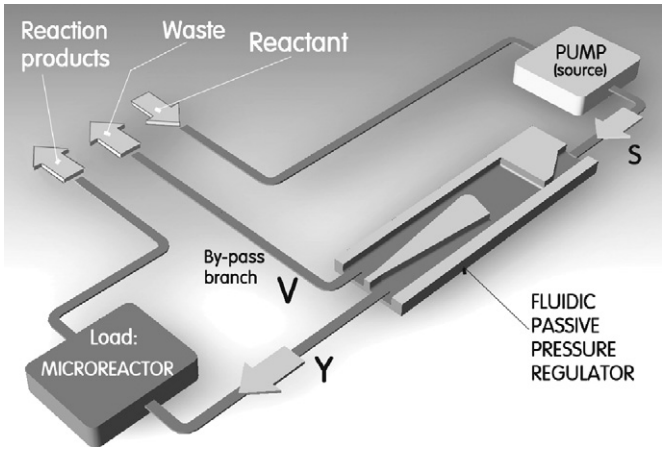

Fig. 7. The usual fluidic circuit design approach, based on the concept of loops, is slightly complicated if the load is a chemical reactor varying the character of the fluid. The source and load loops cannot have simply a common terminal (reaction product should not be re-circulated).

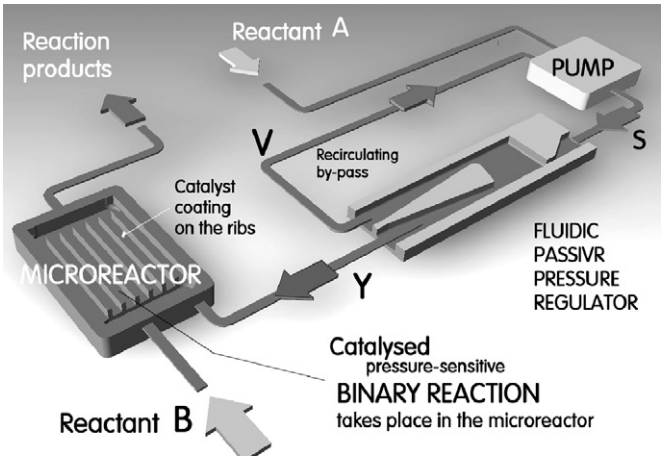

Fig. 8. Although the basic principle of circuit design [14] and use of the regulator is essentially the same as in Fig. 7, the situation is further complicated in the case of a binary chemical reaction.

2. Experimental data

2.1. Model tests

Interestingly, the extraordinary behaviour – with the loading curve converted into the horizontal straight line – was developed without any detailed knowledge of what happens in the interaction cavity, simply by gradually changing the geometry of the model shown in Fig. 8 and watching the consequences. The model was made from PMMA. Its geometry was essentially two-dimensional, with plane cover plates closing the internal cavity on both sides. Nozzle width was $b = 3$ mm and depth, the distance between the cover plates, equal to $h = 8.06b$. In designing the shape, it was believed that the key role in recovering pressure (converted into kinetic energy in the nozzle), it is played by diffusers. That is why the design incorporated in both outlets (output Y as well as vent V) quite long diffusers with small divergence angle 6°. The fluid used in the investigations was at essentially room conditions (Fig. 10).

Based on previous experience with bistable diverter valves the interaction cavity shape was designed so as to make the loading characteristic curve as straight as possible. The curve, in fact, always consists of two arcs with mutually opposed curvatures, positioned one after another. The desirable flatness is achieved by making the curvature radii as large as possible.

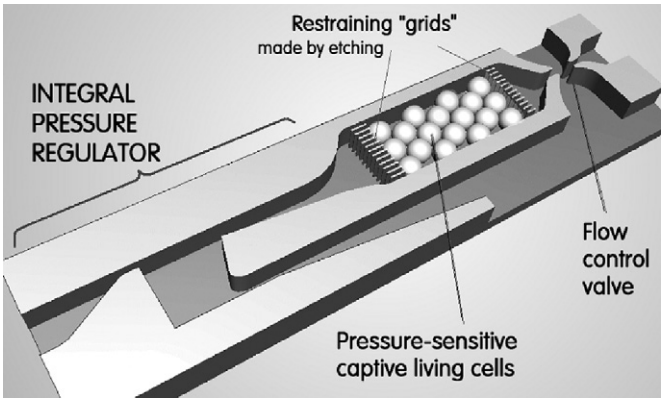

Fig. 9. An example of pressure control in a chamber with captive cells through which passes a varied flow of nutrient liquid – in principle a version of the case from Fig. 7 (the load here involves the colliding-jets control valve [15]).

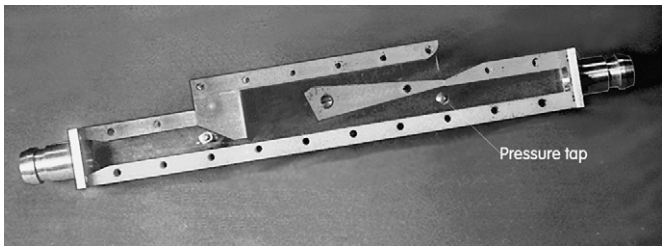

Fig. 10. Photograph of the laboratory tests model used in the development of the geometry of the cavities.

2.2. The slope of the flat loading curve

What was then needed to obtain the desired horizontal loading curve was finding some detail of the geometry that would change of the slope of from the large-curvature-radii curve from the negative value – the curve sloping down with increasing flow rate – as is observed with the initial sharp-edge geometry presented in Fig. 11 into the opposite, positive value. Of course, the initial negative slope may be easily explained by the influence of the internal losses inside the device. These absorb some of the available energy of the fluid (the same effect as in the down-sloping characteristic of the blower in Fig. 3). To make the losses in the output flowpath negative is, of course, not possible. What may be done is adjusting the losses in the other, vent flowpath.

It was established that rounding of the nose of the splitter, making the flow into the vent easier, decreases the slope. Presented in terms of the dimensionless parameters from Fig. 12, the experimental results in Fig. 13 show the effect of various nose radii. Increasing the radius decreases the negative slope. With the nose radius $r = 1.67b$ – in fact the largest that could be actually accommodated between the two tangent straight lines originating in the nose edge – the change in the slope is seen to continue up to reaching the desirable opposite sign. Because of the continuous character if the change, obviously, somewhere between this case and the splitter shapes with small radius r there must be the ideal case of zero slope. Finding it was then just a matter of patient radius variations and repeated measurements of the loading curve. The ideal geometry was found with the radius $r = 1.1b$ with which the regulator device exhibited – at the rather small Reynolds number Re = 2400 – the output characteristics presented in Fig. 14. The loading curve $\pi_Y = f(\mu_Y)$ exhibits almost ideal shape, with the only non-negligible deviations near to the no-spillover state ns (with no flow through the vent V).

Of interest in Fig. 14 is also the small variation of the supply pressure curve $\pi_S = f(\mu_Y)$. This means the fluidic circuits upstream from the regulator are not influenced by whatever changes of hydrodynamic conditions occur in the connected load. This effectively zero fluidic input impedance may itself be a welcome behaviour (in ref. [3] it is described as load-isolator property).

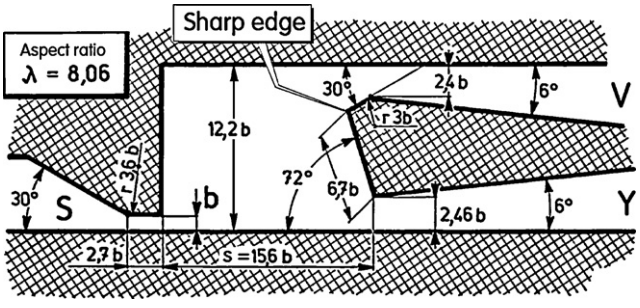

Fig. 11. Geometry of the core part of the model in the initial shape with sharp-edged splitter nose.

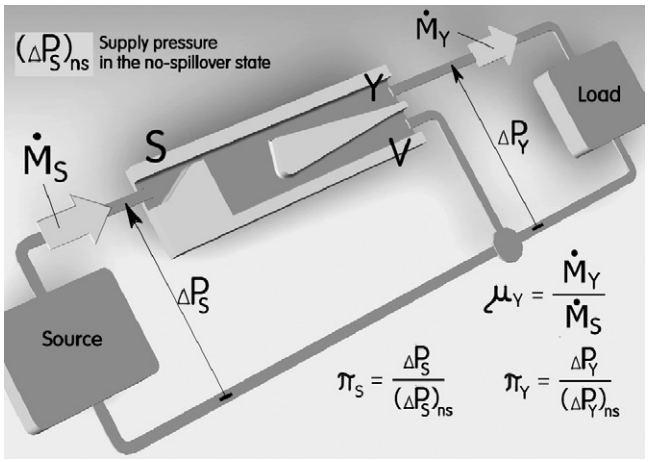

Fig. 12. Measured quantities – flow rates and pressure differences – in the experiments and definition of the dimensionless variables which, thanks to Eulerian similarity [6], replaces the whole family of loading, curves (each valid for particular supply mass flow rate) by a single curve – its universality is, unfortunately, invalidated by Reynolds number effects.

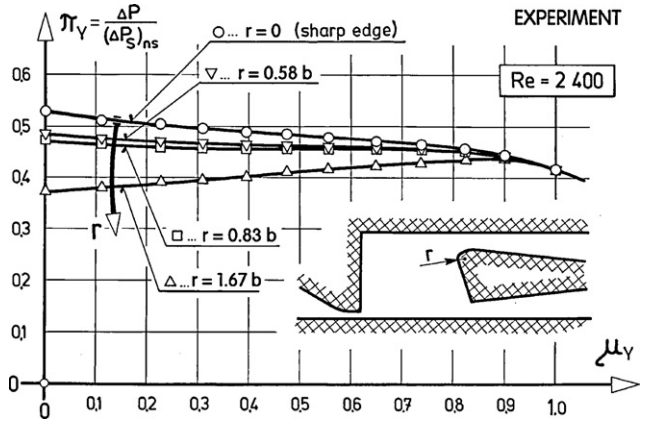

Fig. 13. Experimentally found changes of the loading characteristic – plotted here in relative co-ordinates (Fig. 12) – with gradually increased splitter nose radius r.

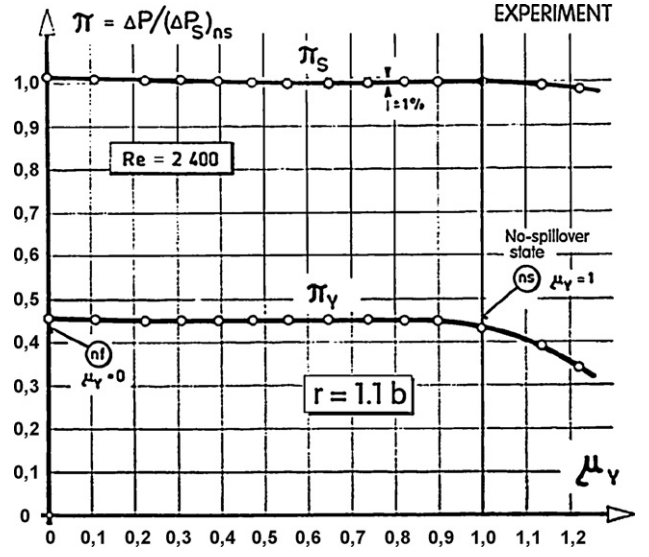

Fig. 14. Output characteristics (the loading curve as well as variations of the supply pressure drop), found for the experimentally determined optimum geometry. Over most of the loading curve, the deviations from perfectly constant pressure are less than mere 2%.

3. Computational studies

3.1. The aim

The absence of a clear explanation why the device possesses the pressure regulating capability was found an unpleasant obstacle when the idea recently received a renewed interest. For the explanation, it was initially planned to build a scaled-up laboratory (model of a size making possible insertion of probes) for investigation of the internal flowfield, it was decided to obtain the information using numerical flowfield solutions. It is necessary to stress the rather special situation. Because of availability of extensive reliable experimental data concerning the outer, "black-box" properties of the device, there was no need for the computations to provide numerically precise results. Instead, it was considered useful just to obtain qualitative explanation of what happens in the regulator cavity at various operating states. The offered alternative presentations of the results by contemporary software made it particularly suitable for this explanatory exercise.

No need of precise numerical results made the computation effort easier. In standard situations, aimed at reproducing exact parameter values, it is necessary to devote a substantial part of the effort to adjustment of solution variables, selection of the best fitting model of turbulence, tuning the numerical constants in the turbulence model, and – in particular, considering the interest in low Reynolds numbers range – a choice of the method for processing the low Re turbulence. This was not considered necessary here.

The solutions were made using commercially available FLUENT software, release 6.3.26, in the 3D version. The solved equations were full three-dimensional Navier–Stokes equations with modified gradient-diffusion term based on the idea of characterising effects of turbulence by a simple scalar quantity – the turbulent viscosity replacing the molecular viscosity in the basic Navier–Stokes equation. This characterisation by a scalar is equivalent to assuming that turbulence is isotropic, its effect identical in all three spatial directions. Turbulence viscosity was computed using *k*-epsilon two-equation model, with the standard model constants as supplied by the software supplier. The regions near to the walls were treated using standard wall functions and the low Re turbulence elsewhere was treated using the RNG approach. The domain was discretised by tetrahedral unstructured mesh, set up using software GAMBIT release 2.4.6. The grid was refined progressively in the course of the solution in regions exhibiting high values of the gradient of velocity magnitude. The working fluid assumed in the computations was the same as the one used in the laboratory tests – air at the room temperature and (in the vent exit) room pressure. To make the flowfield less dependent on the choice of boundary conditions, the geometry of the computation domain was at all three terminals of the device supplemented by additional channel sections of length equal to three channel widths. In the supply terminal the boundary condition was the velocity at the inlet into this upstream extension, the magnitude of the velocity adjusted so as to obtain the same Reynolds number value in the nozzle exit as the value in the laboratory experiments. The other two boundary conditions were the velocity in the downstream extension from the output outlet Y and atmospheric pressure at the vent outlet V. The velocity in Y was adjusted in small steps to different values at different computation runs so as to obtain the data across the whole loading curve of the output characteristic.

3.2. Starting point: the sharp-edge case r = 0

Initially, as the starting point, the geometry of the computational domain was those of the sharp-edged case corresponding to Fig. 11. The computation domain, fully three-dimensional, was of dimensions corresponding to the original laboratory model as shown in Fig. 8, i.e., with nozzle width $b = 3$ mm. The refinement of the discretisation grid progressed in each computation case independently until the number of the finite volumes was ~170,000. The boundary conditions were adjusted so as to keep constant Re = 2400 in the supply nozzle, reproducing the experimental cases presented in Figs. 11 and 12, while the output flow rate boundary condition was gradually increased in small steps. For each of these conditions, the iterations were run (with grid refinement) until the residues of all quantities became lower than 10^{-5}. The resultant pressure differences were evaluated and converted into the dimensionless form using the expression shown in Fig. 12, so that they could be plotted as the data points on output characteristics in Fig. 15, which were obtained by 4th order polynomial fit.

There were 15 computation runs, and therefore the same number of data points defined the loading curve. The overall character of this result – the flat shape of the loading curve and it downwards slope with increasing output flow rate – was in qualitative agreement with the previous experimental data as were presented in Fig. 13.

3.3. Rounded splitter r = 1.5b

In the following series of the computation runs it was decided to investigate the decrease in loading curve slope caused by rounding the splitter nose. The relative rounding radius was chosen to be $r = 1.5b$, i.e., slightly smaller than for the upwards-sloping curve in Fig. 13 but larger than the $r = 1.1b$ for the zero slope case of Fig. 14. The results were plotted together with the sharp-edge case into the same diagram in Fig. 15 where it is apparent that while the slope with the rounded splitter was less steep, it remained negative and did not reach the positive slope value that might be expected on the basis of the experiment. On the other hand, the supply pressure curve $\pi_S = f(\mu_Y)$ was indeed found practically horizontal as shown in Fig. 13.

The general effect of the rounding, the influencing of the character of the loading curve by providing an easier entrance into the vent diffuser, was demonstrated by comparing these two sets of results – and this was considered the fulfilment of the main purpose of the exercise.

The flowfields obtained by these numerical investigations were then investigated in detail with an aim to identify the mechanisms responsible for the character of the loading curve. More disturbing than the imperfect agreement with experimental data (without adjustment of the numerical model variables, an exact agreement

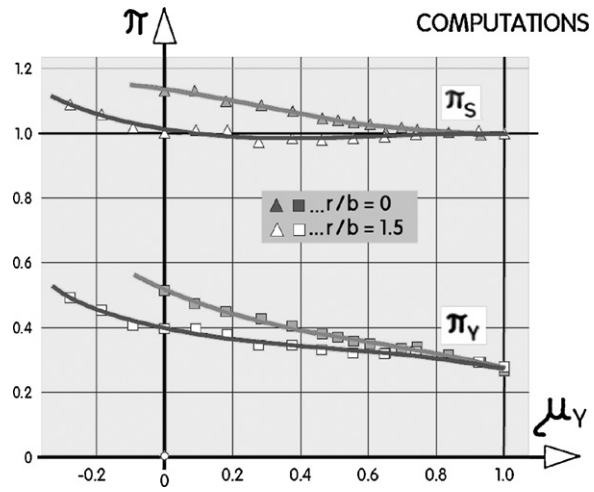

Fig. 15. Output characteristics (both loading curve $\pi_Y = f(\mu_Y)$ and supply pressure curve $\pi_S = f(\mu_Y)$) evaluated by numerical computations for two device geometries: the initial sharp-edge $r = 0$ case and the rounded nose case $r = 1.5b$.

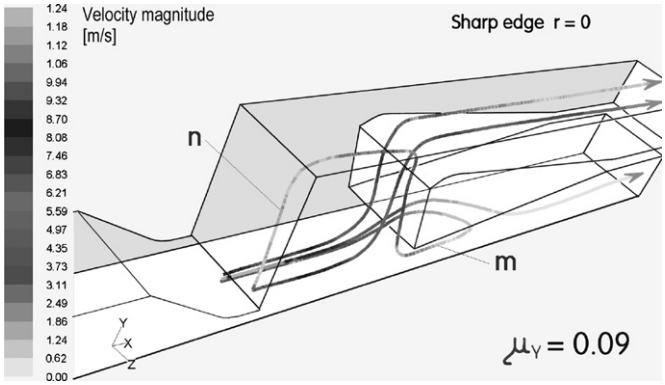

Fig. 16. Pathlines evaluated by computations of the fluid flow in the initial sharp-edge variant show surprising three-dimensionality of the internal flowfield.

could not be expected) was the total invalidation of the basic philosophy of the design. The essentially two-dimensional geometry of the device was from the very outset expected to be reflected also in two-dimensional character of the flowfield – perhaps only weakly influenced by the boundary layers formed on the sidewalls. Initially, such two-dimensional approach was tried, without success, to provide some ideas about the flowfield.

The computations, however, have now shown that the internal flowfield in the device is in reality highly three-dimensional. This is clearly visible, e.g., in the example of computed pathlines presented in Fig. 16. Three pathlines were released from three points located one above another in the vertical line traversing the centre of the nozzle exit. Only one of them – the topmost pathline leaving the cavities through the vent past the sharp edge – actually behaved as expected on the basis of two-dimensional ideas. The middle pathline, leaving through the output terminal, makes a sideways excursion apparently avoiding a large standing vortex located there. This vortex is recognisable from the horizontal loop *m* on the bottom pathline which, after entering the exit diffuser, actually returns back into the interaction cavity. There is follows another, vertical loop *n*. Only after this complex and tortuous path this part of the fluid leaves through the output terminal.

The difficulty of flowing through the vent diffuser is particularly apparent in the zero output flow state for which the computed

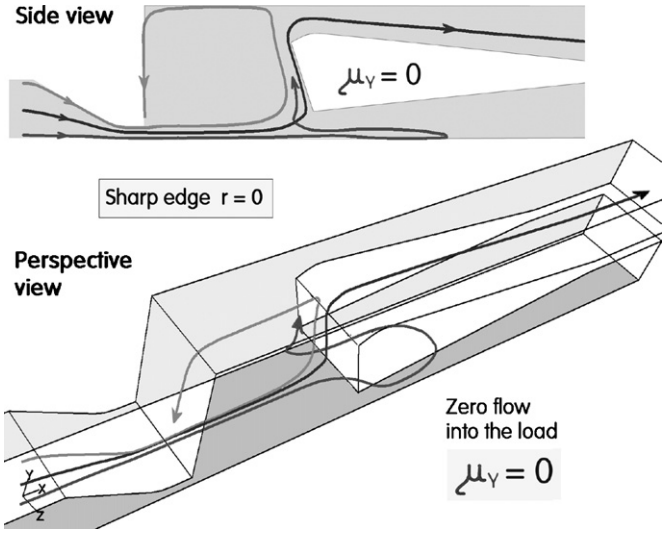

Fig. 17. Computed pathlines for zero output flow state nf in the sharp-edge variant of the device geometry. Entering the vent diffuser is evidently rather difficult and some pathlines reach it only after covering a rather tortuous way, passing through the loop formed in the output diffuser or the large loop in the interaction cavity.

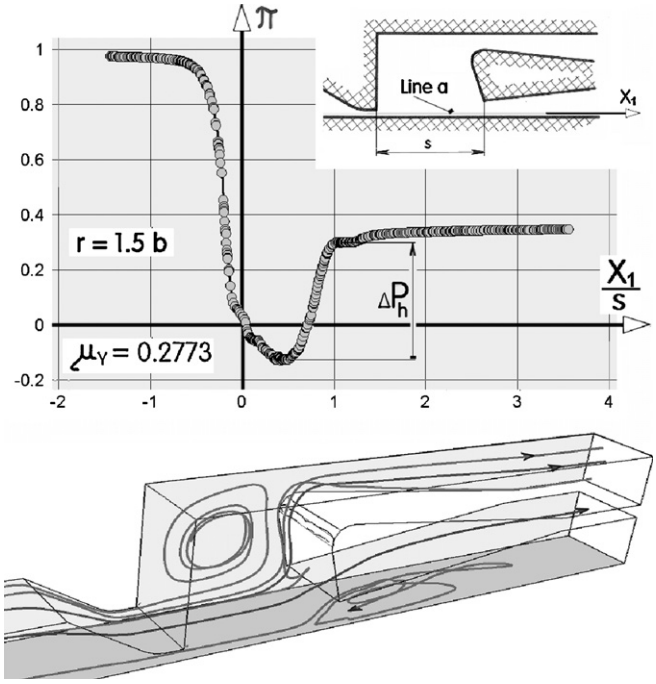

Fig. 18. Top: Computed pressure distribution, presented in relative co-ordinates, along the line a in the regulator element with rounded splitter, in the state with small relative output flow μ_Y. Unexpected fact is the large pressure rise πP_h in front of the entrance into the output diffuser, the pressure recovery in which is actually almost insignificant. Bottom: Corresponding computed pathlines.

pathlines are presented in Fig. 17. Again, the striking feature is the three-dimensionality of some of the flow features.

The pressure changes taking place inside are essential for elucidation of the device behaviour. They are also important from the practical point of view. The device belongs into the jet-type category of fluidic devices dependent on dynamic phenomena in fluid accelerated in the nozzle. It is essential for energetic efficiency of the device to recover as much as possible of the pressure by re-conversion from the kinetic energy before the fluid leaves the cavities. It was with this aim in mind that the device was provided with the two diffusers occupying a substantial proportion of the available space. The diffuser in the vent exit, rarely if ever used in other known fluidic devices, is there actually with the intention to generate the pressure rise that was considered essential for adjusting the degree of ease with which fluid can leave through the vent.

An interesting example of what may be learned about the pressure changes is given by the computed pressure distribution in the upper part of Fig. 18. The local static pressure values, for the $r = 1.5b$ rounded nose case at the flow rate into the output slightly more than one quarter of what is supplied into the nozzle, were evaluated along the line a shown in the inset at the right-hand upper corner of this picture. The data are plotted in relative co-ordinates: the pressure values are – according to Fig. 12 – related to the supply pressure difference in the no-spillover state and the distances are related to the splitter distance *s*. The distances are measured from the nozzle exit. The dramatic pressure decrease in the streamwise direction for the negative distance values is obviously due to the pressure energy conversion inside the nozzle into the kinetic energy. Downstream from the exit, the pressure values on the line a are negative, lower than those in the vent exit, which may be interpreted as the effect of the pressure rise in the part of the flow leaving through the vent. It is what happens further downstream along the line a that is unexpected. Traditional view of the processes taking place in fluidic jet-type device expects the jet flow

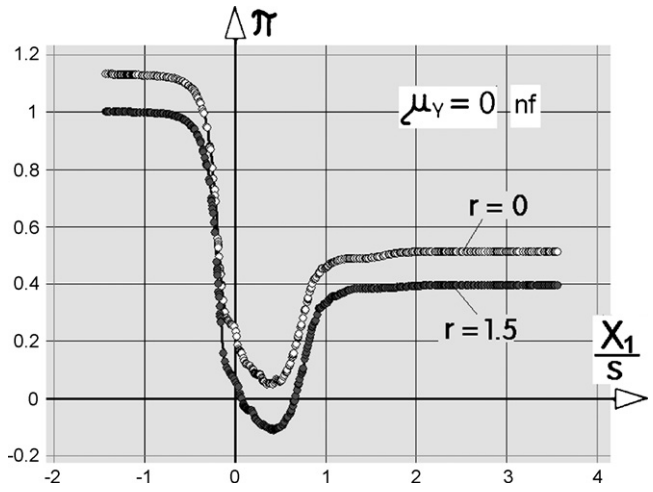

Fig. 19. Pressure distributions along the line a in the two versions of the regulator: one with the sharp splitter edge $r = 0$, the other with the edge rounded. Both computed for all the flow passing through the vent, where the effect of the entrance into the vent diffuser is most pronounced.

to be isobaric, with the pressure recovery due to the pressure rise taking place inside the exit diffuser further downstream. The computed results in Fig. 18 do not show this to be the case. The pressure rise in the diffuser, at $X_1 > s$, is seen to be of little importance. The perspective view of the computed pathlines in the bottom part of Fig. 18 may explain the poor performance of the output diffuser as a consequence of the separated recirculation flow filling a considerable part of the diffuser. What pressure recovery takes place is seen in the top part of Fig. 18 due to the pressure rise ΔP_h in front of the entrance into the output diffuser. There is little doubt that this rise is caused by the mechanism recently identified under similar conditions in ref. [7]. It is probably associated with the Ringleb's idea [8] of trapped vortex – several times seemingly disproved (e.g., [9]) and yet later resuscitated, e.g., in the form of vortex trapped in a cornice-shaped cavity on the top surface of an airfoil, known as the "Kasper vortex" [10], a subject of current research efforts [11,12].

Analogous pressure distributions presented in Fig. 19 for the zero out put flow rate (state nf) in the two cases $r/b = 0$ and $r/b = 1.5$ show remarkable mutual similarity. The difference is merely in their vertical separation. Evidently, the unwelcome negative slope in Fig. 13, more pronounced in the $r = 0$ case is associated with the stronger shift upwards, i.e., a higher pressure in the interaction cavity – no doubt because of the more difficult entry into the vent diffuser.

The obvious lesson learned from these results is the better approximation to the desirable zero loading curve slope may be obtained by making the vent flow even more easy.

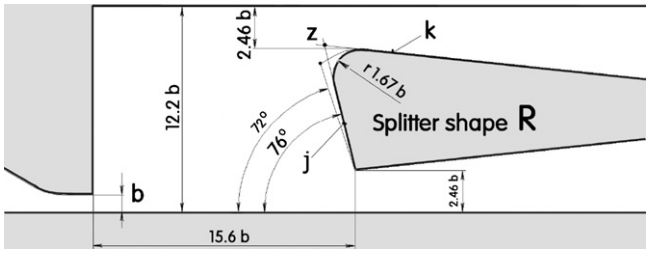

Fig. 20. In an attempt to obtain a positively sloping computed loading characteristic, in the third tested geometric alternative R of the splitter shape, the entrance into the vent was made easier by increasing the splitter head angle to 76° and rounding with radius $r = 1.67b$ the whole triangular, region between the lines j and k (intersecting at an angle 70°) which, when extended, meet in their intersection point z.

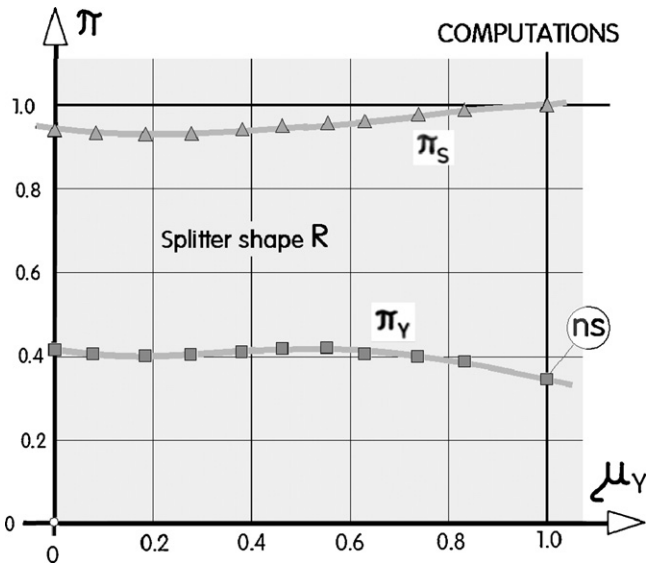

Fig. 21. Loading curve $\pi_Y = f(\mu_Y)$ and supply pressure curve $\pi_S = f(\mu_Y)$ in the output characteristics, evaluated from numerical computations of the device with splitter shape R. The loading curve is perhaps the nearest approximation by the performed numerical solutions to the ideal horizontal straight line of a pressure regulator.

3.4. Splitter shape R: yet easier entrance into the vent

Since the original shape of the splitter, as presented in Fig. 11, defined by the two straight lines intersecting in the sharp-edge point does not allow significant increase in the rounding diameter r, beyond the $r/b = 1.5$ value, it was decided to make the entry into V easier by increasing the slope of the splitter head wall, which at the initial value 72° (Fig. 11) obviously turns quite rearwards the part of the flow not entering the output diffuser. As shown in Fig. 20, the angle was increased to 76°. This made the upper one of the two intersection lines even shorter. The rounding was therefore made differently: the rounded part of the splitter is now positioned between the two lines j and k, which – when extrapolated – intersect in the point z.

With the resultant splitter geometry R, the loading curve in relative co-ordinates $\pi_Y = f(\mu_Y)$, as presented in Fig. 21, exhibits a very good approximation to the desirable horizontal straight line shape – apart from the immediate neighbourhood of the no-spillover state ns (which is the weak point of the regulator accuracy also according to the experimental data presented in Fig. 14). The larger deviation from the load-isolator property (i.e., from the shape of the ideal supply pressure curve $\pi_S = f(\mu_Y) = 1.0$) is inconsequential in the present context.

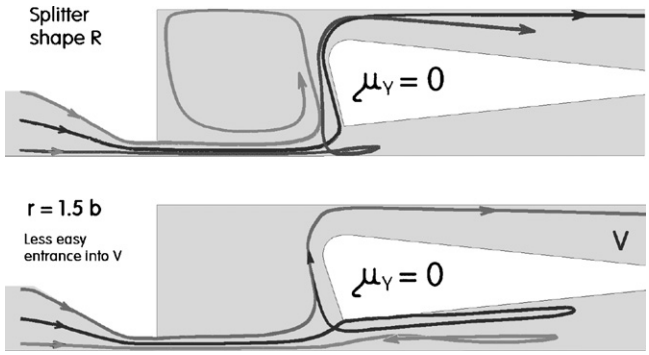

Fig. 22. Comparison of side views of computed three pathlines released, under the same conditions, into the regulator with splitter shape R (top) and the $r/b = 1.5$ rounded splitter geometry (bottom). The zero output flow state nf makes most pronounced the differences between the entrance into the vent diffuser.

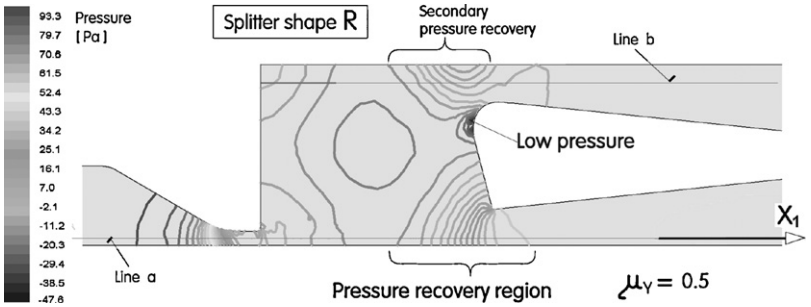

Fig. 23. Pressure field in the mid-plane computed for the R shape variant in the state with 50% spillover into vent V, i.e., exactly half-way between the extreme ns and nf states.

Certain idea about the achieved ease of entry into the vent may be gained from the sideways views of the flowpaths in Fig. 22, computed under exactly identical nf conditions (i.e., no flow through the load). While in the earlier $r/b = 1.5$ rounded shape cavity only one of the three pathlines managed to escape through the vent, in the splitter shape R case two pathlines left there within the same number of pathline computation steps.

4. Findings

4.1. Three-dimensionality

Of the two main lessons learned from the performed computational exercise, the first one is of considerable importance for fluidics and microfluidics in general. It is the surprising degree of three-dimensionality. Although quite often made, the simple one-dimensional calculations (or better termed, estimations) of the velocities and pressure conditions based on the size of channel cross sections – and an idea of the flow filling the sections – is inapplicable in the flow where the jets enter the collectors only to be forced to flow back. It should be said that this rather deep penetration into the collector was the more unexpected in the present case the larger is here the splitter distance $s = 15.6b$. This is twice and perhaps even more than the usual distance in most jet-type fluidic devices (cf. e.g., [13]) where the penetration energy must be correspondingly more effective.

The design of the discussed pressure regulator devices, guided by the idea of the ease of entry into the vent, is therefore quite difficult because before even entering the vent diffuser the fluid flow has to follow a rather complicated paths, sometimes with loops (Figs. 14–16) which – Fig. 18 – may be entangled in a complex manner.

4.2. Pressure recovery mechanism

The character of the internal flow depends very much upon the action of pressure forces. An example of generic pressure distribution, presented in terms of isobars (drawn in the mid-plane, i.e., at distance $h/2$ between the side cover plates) is provided in Fig. 23. The consequences for the pressure changes roughly in the direction of the flows is seen in Fig. 24 where, in addition to the pressure along the line a (passing through the middle of the nozzle) as in Figs. 16 and 17, there are also pressure distribution along the line b (Fig. 23 – passing through the middle of the entrance into the vent diffuser).

Obviously, as already noted above, the almost no pressure variations are found in the components – diffusers – that were included just in order to generate the pressure rise. Of course, no changes are expected in the inactive diffusers – as seen from the horizontal line distributions for the output diffuser in the nf regime and the vent diffuser in the ns state (Fig. 24). Nevertheless, even in the

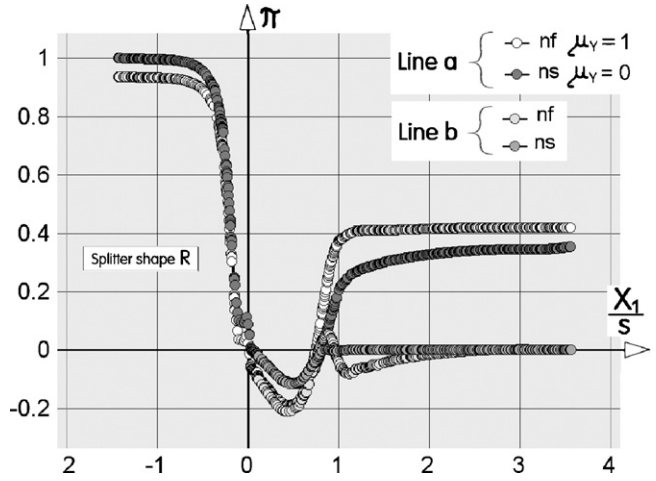

Fig. 24. Computed pressure distributions along both line a as well as line b (as shown in Fig. 23) in the extreme ns and nf states in the regulator device with splitter shape R.

active diffusers handling the full flows the rise is much smaller than the recovery by the mechanism according to ref. [7]. This pressure increase takes place in the impingement regions, in the corners of the interaction cavity where the wall-jets following the walls are forced to change their direction. Also the pressure rise of the flow passing through the vent is due to the secondary pressure recovery region of the same character (Fig. 23).

Quite interesting is also the low pressure region seen in Fig. 23 near the splitter nose. It is doubtless the pressure force that holds, like the Coanda effect, the wall jet attached while it is turned into the vent collector and this makes it an important factor in designing the shape for an easy entrance into the vent.

5. Conclusions

Numerical flowfield solutions were used for a not very common purpose of elucidating operation of a device that was already developed to satisfactory level by purely empirical procedure. The emphasis on the qualitative character of the computation results made unimportant search for precise reproducibility of numerical values. It was especially the post-processing offered by the software that made possible interesting detailed studies of features in a way that would be very difficult to perform by experiments – for example following the pathlines into their complex entangled loops.

The discussed device offers several useful application opportunities that has been so far ignored, but was a subject of a new interest. It belongs into the jet-type category of fluidic devices dependent on dynamic phenomena in fluid accelerated in the nozzle and this makes important investigation of the pressure recovery

mechanisms. Rather surprisingly, the mechanism was found to be quite different (not taking place in the diffusers) than the ideas that were followed in the original device design.

Acknowledgments

Gratefully acknowledged is the financial support by the grant IAA200760705 and by the research plan AV0Z20760514 provided by Grant Agency of the Academy of Sciences of the Czech Republic. Another partial support was obtained from the grant no. 101/07/1499 donated by the Grant Agency of the Czech Republic.

References

[1] R.L. Moore, D.M. Hanlon, B.G. Lipták, Regulators-pressure, Part 5.6 in Instrument Engineer's Handbook, 3rd. Edition, CRC Press, 2005, p. 650.
[2] V. Tesař, Obtokový regulátor tlakového spádu (By-pass type regulator of pressure drop – in Czech), expired Czechoslovak Patent no. 183 461 (1976).
[3] V. Tesař, No-moving-part pressure regulator/load-isolator fluidic element, Fluidics Quarterly 11 (September (3)) (1979) 43.
[4] R.L. Woods, R.-J. Tseng, A fluidic low output impedance device, in: Proceedings of FLUCOME '85, Fluid Control, Mechanics, Measurement, and Visualisation Symposium, Tokyo, 1985, p. 229.
[5] V. Tesař, Microfluidic systems for combinatorial chemistry, in: Dongqing Li (Ed.), Encyclopedia of Microfluidics and Nanofluidics, Springer, Heidelberg, 2008, p. 1221, ISBN: 978-0-387-48998-8.
[6] V. Tesař, Pressure-Driven Microfluidics, Artech House Publishers, Norwood, MA 02062, USA, 2007, ISBN: 1596931345.
[7] V. Tesař, Mechanism of pressure recovery in jet-type actuators, Sensors and Actuators A Physical 152 (2009), p. 182.
[8] F.O. Ringleb, Separation control by trapped vortices, in: G.V. Lachman (Ed.), Boundary Layer and Flow Control, Pergamon Press, Oxford, UK, 1961.
[9] E.W. Kruppa, A wind tunnel investigation of the Kasper vortex concept", American Institute of Aeronautics and Astronautics, Paper # 115704, 1977.
[10] J. Cox, The revolutionary Kasper wing, Soaring, vol. 37, 1973, p. 20.
[11] *VortexCell2050 project*, funded by the European Commission within its FP6 Programme, contract number, AST4–CT–2005-012139, www.vortexcell2050.org.
[12] B. Protas, Vortex dynamics models in flow control problems, Nonlinearity 21 (2008) 203.
[13] V. Tesař, et al., Experimental investigation of a fluidic actuator generating hybrid-synthetic jets, Sensors and Actuators A 138 (2007) 213.
[14] V. Tesař, Fluidic circuits, in: W.B.J. Zimmerman (Ed.), Microfluidics: History, Theory, and Applications, Springer-Verlag, Wien, New York, 2006, p. 255 (Chapter 15).
[15] V. Tesař, Microfluidic turn-down valve, Journal of Visualization 5 (3) (2002) 307.